Received February 11, 2022, accepted February 24, 2022, date of publication February 28, 2022, date of current version March 3, 2022.

Digital Object Identifier 10.1109/ACCESS.2022.3155120

Wideband Dual-Circularly Polarized Antennas Using Aperture-Coupled Stacked Patches and Single-Section Hybrid Coupler

SON XUAT TA[1], VAN CUONG NGUYEN[1], BANG-TAM NGUYEN-THI[1], THAI BAO HOANG[1], AN NGOC NGUYEN[2], (Member, IEEE), KHAC KIEM NGUYEN[1], AND CHIEN DAO-NGOC[1], (Senior Member, IEEE)

[1]School of Electronics and Telecommunications, Hanoi University of Science and Technology, Hanoi 100000, Vietnam
[2]Faculty of Electronics and Telecommunication, University of Engineering and Technology, Vietnam National University, Hanoi 100000, Vietnam

Corresponding author: Son Xuat Ta (xuat.tason@hust.edu.vn)

ABSTRACT This paper presents a dual-circularly polarized (dual-CP) antenna with simple configuration, low-profile, and wide bandwidth. Its primary radiating element is an aperture-coupled patch loaded with a stacked patch for a wide operational bandwidth. A single-section hybrid coupler is utilized as a feeding structure of the antenna to generate dual-CP radiation. Different from the priors normally requiring both wideband radiator and wideband feeding structure, this work demonstrates that the wideband dual-CP radiation can be obtained by combining a wideband radiator and a conventional hybrid coupler. A design operating at the center frequency of 5.5 GHz has been fabricated and tested. The measurements result in a −10-dB reflection coefficient bandwidth of 30.0% (4.66 – 6.31 GHz), a 10-dB isolation bandwidth of 30.9% (4.66 – 6.35 GHz), a 3-dB axial ratio (AR) bandwidth of 29.1% (4.70 – 6.30 GHz), and a realized broadside gain of 5.5 – 7.05 dBic. For a more robust dual-CP radiation, a low-sidelobe 4 × 4 element array of the proposed antenna has been designed, fabricated, and measured. Compared to the single element design, the array prototype yields similar impedance and 3-dB AR bandwidths, but a higher isolation. The measurements on the array prototype result in an isolation of ≥14 dB, a peak gain of 16.3 dBic, a side-lobe level of ≤−20 dB, and a cross-polarization of ≤−16 dB across the frequency range of 4.7 – 6.3 GHz (29.1%).

INDEX TERMS Dual circular polarization, aperture-coupling, stacked patch, single-section hybrid coupler, wideband, array, side-lobe level.

I. INTRODUCTION

In modern wireless systems, circularly polarized (CP) wave is used as a powerful technique to mitigate multipath interference, polarization mismatch, and the Faraday effect. As a result, CP antennas [1] have been developed widely for several applications in radio frequency identification [2], global positioning system [3], wireless local area network (WLAN) [4], satellite communications [5], [6], synthetic aperture radar [7], and so on. Moreover, dual-CP antennas, which can generate both right- and left-hand CP (RHCP and LHCP) radiations, are expected for not only polarization diversity but also frequency reuse [8].

The associate editor coordinating the review of this manuscript and approving it for publication was Qi Luo.

Microstrip patch antennas [9] are a preferred choice to construct dual-CP systems because of their features, such as low-profile, simple fabrication, and low cost. In order to generate the dual-CP radiation, the conventional patch antennas [10]–[12] are commonly fed by the single-section hybrid couplers, which provide either RHCP or LHCP depending on the port excitation. Alternatively, both RHCP and LHCP can be generated when a single microstrip-line [13] traversed a cross-slotted aperture in a serial manner for coupling with the microstrip patch. Furthermore, a dual-CP patch antenna [14] can be realized by exploiting even and odd modes in a coplanar waveguide transmission line. In addition [15], a dual-CP radiation was achieved at WLAN frequency band (2.4 – 2.485 GHz) when a truncated-corner square patch was fed by a square ring slot with two orthogonal microstrip-lines. Since these dual-

CP antennas utilized a conventional patch as the primary radiating element, they suffer a common drawback of narrow operational bandwidth. Here, the operational bandwidth is defined by the following specifications, namely reflection coefficients ≤ -10-dB, port-to-port isolation ≥ 10-dB, and axial ratio (AR) ≤ 3-dB.

In the last decade, several approaches have been devoted to broaden the operational bandwidth of dual-CP patch antennas. By using stacked patches and a two-section hybrid coupler, a dual-CP antenna array [16] enlarges the operational bandwidth up to 14.7% for satellite communications in the X band. An air-substrate patch antenna [17] is fed by a four cross slots via a microstrip-line with multiple matching segments to achieve a dual-CP bandwidth of 16%. In [18], a square patch antenna is surrounded by 12 parasitic metal plates to obtain an operational bandwidth of 16.5%. Another way to improve the operational bandwidth of a dual-CP patch antenna is to combine a broadband radiator and a broadband feeding network to generate orthogonal fields. As an example, a patch array [19] uses a sequentially rotated feeding network to provide a RHCP bandwidth of 12.5% (4.95 – 5.61 GHz) and LHCP bandwidth of 14.7% (5.05 – 5.85 GHz). Although these approaches have improved the dual-CP radiation bandwidth considerably compared to what the conventional designs provide, their bandwidths are still limited within 17%.

Besides the preferable microstrip patch type, many other types of antenna have been developed for the dual-CP systems. A cavity-backed ring-slot antenna [20] is loaded with an artificial magnetic conducting reflector to produce dual-CP radiation, and to have a compact size, and low profile. In [21], a traveling wave series-fed patch array is fed by a microstrip-line through proximity coupling for a dual-CP radiation at 10 GHz. In particular, the dual-port feeding helps to control the direction of the traveling wave to generate either RHCP or LHCP. In another effort, a dual-CP antenna with an electrically small size of $ka = 0.94$ [22] is realized by utilizing multilayer stacked near-field resonant parasitic elements. In addition, a high-gain dual-CP radiation can be realized by constructing a Fabry-Perot antenna [23], [34], [35], which consists of a dual linearly polarized (dual-LP) patch antenna and a polarization conversion metasurface. Since the aforementioned dual-CP antennas targeted a compact size [20], [22] or employed conventional patch as the primary radiating elements [21], [23], [34], their operational bandwidths are less than 5% only.

Recently, several wideband dual-CP antennas have been presented. In one direction, the wideband and low-profile features of metasurface are exploited to construct wideband dual-CP antennas in [24], [25]. These designs, however, possess a drawback of metasurface antenna, which is a large footprint. In another attempt [26], four printed dipoles with two balun-included feeding networks are incorporated with a three-section quadrature hybrid coupler to achieve a dual-CP radiation with an operational bandwidth of >66%.

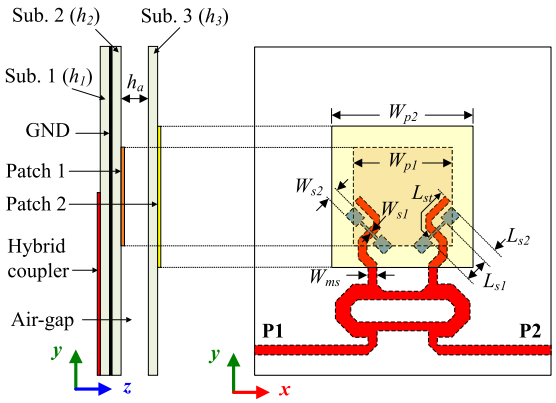

FIGURE 1. Geometry of the dual-CP aperture-coupled stacked patch antenna.

In addition, crossed dipoles loaded with a circular patch [27] are excited in quadrature for wideband dual-CP at the L-band satellite applications. In [28], a magnetoelectric (ME) dipole antenna with four V-shaped patches and four V-section columns is fed by two Γ-shaped probes for a 41.9% dual-CP bandwidth. For the efficient broadside radiation, the antennas in [26]–[28] require a distance of $0.25\lambda_c$ between the radiator and reflector, which causes a bulky configuration.

In this paper, we propose a low-profile dual-CP antenna with wideband operation and its low-sidelobe 4×4 element array. Differing from the mentioned techniques, our proposed antenna employs a single-section hybrid coupler as the feeding structure to achieve dual-CP radiation. Meanwhile, the aperture-coupled stacked patches are used to broaden the operational bandwidth. The proposed antennas are arrayed in a 4×4 layout to strengthen the robustness of dual-CP radiation, i.e., increasing broadside gain, reducing sidelobe level (SLL), and enhancing port-to-port isolation. The antenna features are computationally demonstrated by using ANSYS Electronics Desktop and confirmed experimentally.

II. WIDEBAND DUAL-CIRCULARLY POLARIZED ANTENNA

A. GEOMETRY

Fig. 1 shows the geometry of the proposed antenna. It is composed of a single-section hybrid coupler, two square patches (patch 1 and 2), a ground plane (GND) with two orthogonal I-shaped slots, and three substrates (Subs. 1–3). The hybrid coupler is printed on the bottom side of the Sub. 1 (RO4003C, $\epsilon_r = 3.38$ and $\tan\delta = 0.0027$). Patch 1 and 2 are placed on the top sides of the Subs. 2 and 3, respectively. FR4 ($\epsilon_r = 4.4$ and $\tan\delta = 0.02$) is used as Subs. 2 and 3. The GND is sandwiched between the Subs. 1 and 2 with no air-gap, whereas the Sub. 3 is stacked above the Sub. 2 at a height h_a. Patch 1 is coupled with the hybrid coupler via the two orthogonal I-shaped slots embedded in the GND. The proposed antenna is characterized by using the ANSYS Electronic Desktop for a wideband dual-CP radiation at the center frequency of about 5.5 GHz. The design parameters are given in Table 1.

TABLE 1. Optimized design parameters of the proposed antenna.

Parameter	Value (mm)	Parameter	Value (mm)	Parameter	Value (mm)
W_{ms}	1.1	W_{s1}	0.3	W_{s2}	1.5
L_{s1}	3.0	L_{s2}	1.8	L_{st}	5.9
W_{p1}	12	W_{p2}	17.3	h_a	3.0
h_{s1}	0.508	h_{s2}	0.6	h_{s3}	0.6

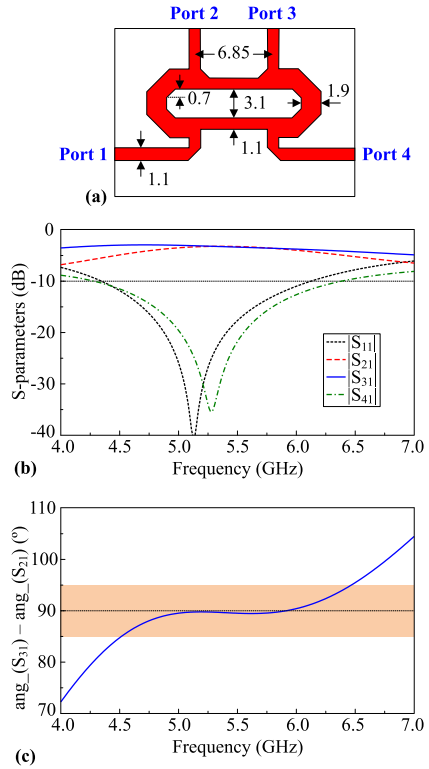

FIGURE 2. (a) Geometry of the hybrid coupler (unit in mm), (b) simulated S-parameters and (c) phase difference between S_{21} and S_{31}.

B. HYBRID COUPLER

In order to generate the dual-CP radiation, the proposed antenna utilizes a conventional quadrature hybrid coupler [29] as the feeding network. Based on the basic configuration, the branch-line coupler is compensated for the center frequency of 5.5 GHz and the RO4003C substrate ($\epsilon_r = 3.38$, $tan\delta = 0.0027$, $h_1 = 0.508$ mm), and slightly modified for a more compact deployed area. The feeding network is numerically characterized by the ANSYS Electronic Desktop, and its performances are illustrated in Figs. 2(b) and 2(c). It is observed that the coupler has a good performance in the frequency range from 5 GHz to 6 GHz, i.e., the reflection coefficients (e.g., S_{11}) are <-10 dB; the isolation (S_{41}) is >10 dB with a peak of 35 dB at 5.3 GHz; S_{21} and S_{31} have a nearly equal magnitude (3.2 ± 0.3 dB) and a $90° \pm 0.5°$ phase difference. The performance of the coupler degrades when the examined frequency range increases. S_{21} and S_{31} have a $90° \pm 5°$ phase difference at 4.5 – 6.5 GHz.

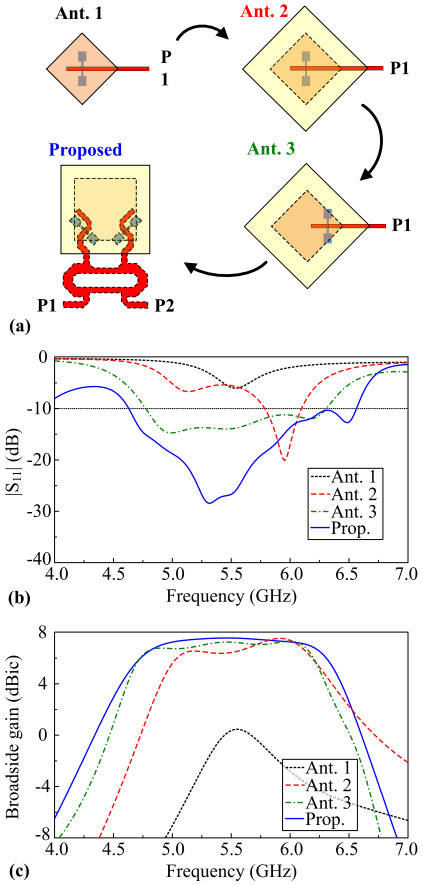

FIGURE 3. (a) Design evolution of the wideband dual-CP antenna; (b) simulation S_{11} values and (c) broadside realized gains for different configurations.

C. DESIGN EVOLUTION

The proposed antenna is a combination of a conventional hybrid-coupler and aperture-coupled stacked patches to generate a wideband dual-CP radiation. For a better illustration of the antenna operation, Fig. 3 shows the design evolution and corresponding performance for each step. The initial design is a conventional aperture-coupled patch antenna (Ant. 1). To broaden the bandwidth, Ant. 1 is loaded with a stacked patch to create Ant. 2. The aperture position of Ant. 2 is shifted forward one patch corner (Ant. 3) to improve the impedance matching. The proposed design is formed by adding an aperture and the hybrid coupler to Ant. 3. The design parameters of all configurations are same as the final antenna.

Figs. 3(b) and 3(c) show the S_{11} values and broadside realized gains of the four configurations. Since Ant. 1 is the conventional aperture-coupled patch antenna and not fully optimized, it yields a resonance at 5.54 GHz with $S_{11} = -6$ dB only and a gain of 0.44 dBi. By loading a stacked patch, Ant. 2 yields two resonances at 5.14 GHz and 5.95 GHz and a realized gain of >6 dBi in the frequency range of 5.04 – 6.19 GHz. In the case of Ant. 2, the aperture is located at the center, the patch 1 acts as a feeding patch, and therefore,

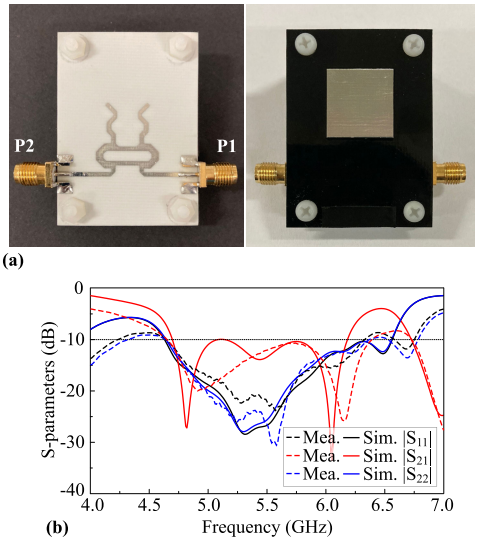

FIGURE 4. (a) Fabricated sample of the proposed antenna and (b) its S-parameters.

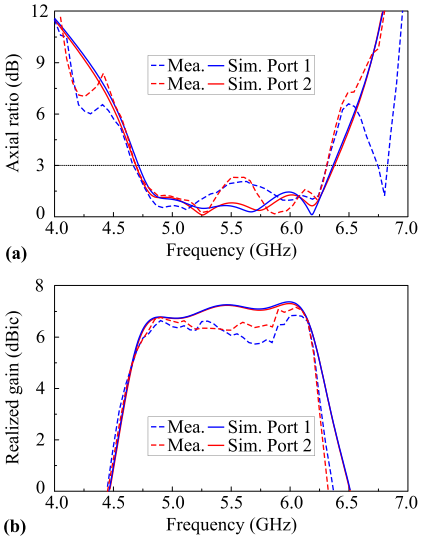

FIGURE 5. (a) AR and (b) broadside gain of the antenna prototype.

its resonance is not appeared. By tuning the aperture position, we can excite three resonances generated by the two patches and aperture slot, and consequently, achieving a wideband operation [30]. This is illustrated by the performance of Ant. 3, which yields a −10 dB bandwidth of 27.8% (4.77 – 6.31 GHz) with three resonances at 5.0 GHz, 5.5 GHz, and 6.18 GHz. Moreover, Ant. 3 achieves a broadside realized gain of 6.3 – 7.55 dB within its bandwidth. Due to presence of the hybrid coupler as feeding structure, the proposed antenna achieves a broader impedance bandwidth and a dual CP radiation. As shown in Figs. 3(b) and 3(c), the proposed design achieves an impedance bandwidth of 34.3% (4.64 – 6.56 GHz) and a broadside realized gain of 5.7 – 7.3 dBic. The dual-CP performance of the proposed antenna will be presented later in the next subsection.

D. FABRICATION AND MEASUREMENT

For verification, the proposed wideband dual-CP antenna was fabricated and measured. Fig. 4(a) shows an antenna prototype with overall size of 36 mm × 50 mm × 4.7 mm ($0.56\lambda_{min} \times 0.77\lambda_{min} \times 0.07\lambda_{min}$, where λ_{min} is the free space wavelength at the lowest operating frequency). All components, including feeding structure and stacked patches, were realized by using the printed circuit board (PCB) technology. The three PCB components were combined together by using plastic posts and screws. Two 3.5-mm sub-miniature version A (SMA) connectors are used as the microstripline-to-coaxial adapters. Note that the size of the fabricated prototype was chosen to be compatible with the available SMA connectors, plastic posts and screws. The simulation results indicate that the antenna size can be reduced to 30 mm × 30 mm × 4.7 mm ($0.46\lambda_{min} \times 0.46\lambda_{min} \times 0.07\lambda_{min}$) with a negligible degradation in performance.

The S-parameters of this antenna prototype were measured by using a vector network analyzer and compared to the simulation results in Fig. 4(b). The measurement results show a −10 dB reflection coefficient bandwidth of 30.0% (4.66 – 6.31 GHz) for both ports, while the simulated impedance bandwidth is 33.9% (4.65 – 6.55 GHz). The measured bandwidth for isolation >10-dB was 30.9% (4.66 – 6.35 GHz), which is comparable with the respective simulation result of 27.2% (4.7 – 6.18 GHz). A slight difference between the measurement and simulation results could be caused by the undesired air gaps between the stacked substrates.

The radiation characteristics of the antenna prototype was measured in a tapered anechoic chamber (provided by Microwave Vision Group at ACE Antenna Co., Ltd, Ha Nam Province, Vietnam). Fig. 5 shows the AR and broadside gain values. Due to the structure's symmetry, both the excitations at Port 1, 2 generate nearly identical values of ARs and gains. As shown in Fig. 5(a), the measurement result shows a CP bandwidth of 29.1% from 4.7 to 6.3 GHz (AR ≤3 dB for both ports excited), which is relatively close to the simulated CP bandwidth result of 30% (4.71 – 6.37 GHz). As shown in Fig. 5(b), within the CP bandwidth, the measured gain is 5.5 – 7.05 dB, while the simulated gain is in the range of 5.7 – 7.3 dB. The measured gains are slightly smaller than the simulated values, which could be attributed losses caused by the SMA connectors, plastic posts, and screws.

Fig. 6 shows the 5.5 GHz radiation patterns of the proposed antenna. Simulation and measurement results agree that the proposed antenna has achieved a good dual-CP radiation, with Port 1 for RHCP and Port 2 for LHCP. Moreover, the antenna prototype has a highly symmetrical radiation pattern with half-power beamwidth (HPBW) of 65° ± 5°, cross-polarization level of <−15 dB at the broadside-direction, and a front-to-back (F-B) ratio of >15 dB. Because the radiation pattern of the prototype is stable across the operational bandwidth, only the radiation pattern at 5.5 GHz is shown for brevity.

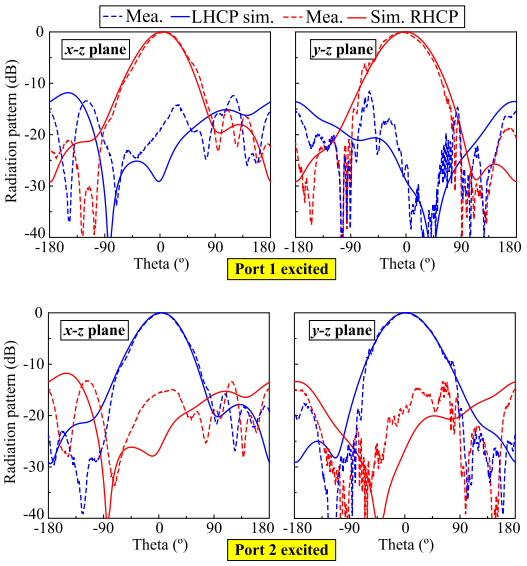

FIGURE 6. 5.5-GHz radiation pattern of the antenna prototype.

TABLE 2. Comparison of the wideband dual-CP antennas.

Ant.	Size (λ_{min})	Feeding structure	Operational BW (%)	Isolation	Gain (dBic)
[17]	0.81×0.81 ×0.17	1 MS-line + 4 cross-slots	16.0	>10 dB	9.6
[18]	0.53×0.53 ×0.05	1-section hybrid coupler	8.9	>20 dB	6.6
[24]	0.70×0.70 ×0.07	2 MS-lines + 1 cross-like slot	12.2	>15 dB	7.1
[25]	0.71×0.71 ×0.04	2 MS-lines + 1 ring slot	31.3	>10 dB	7.0
[26]	0.56×0.56 ×0.15	3-section hybrid coupler	79.7	N/A	9.3
[27]	1.0×1.0 ×0.16	Narda 4032C coupler	37.0	>40 dB	9.0
[28]	1.1×1.1 ×0.26	2 Γ-shaped probes	41.9	>10 dB	10.0
Prop.	0.77×0.56 ×0.07	1-section hybrid coupler	29.1	>10 dB	7.3

λ_{min} is the free-space wavelength referring to the lowest operational frequency. The operational bandwidth (BW) is specified with reflection coefficients ≤ -10-dB, AR $\leq$ 3-dB, and port-to-port isolation $>$ the specified values. N/A is not available.

Table 2 shows a comparison between the performance of the proposed antenna and those of the existing wideband dual-CP designs. It is observed that the proposed antenna has a simpler configuration and a considerably wider operational bandwidth as compared to most of the dual-CP antennas with low-profile, e.g., [17], [18], [24], [25]. Differing from the prior designs [26]–[28] that require both a wideband radiator and a wideband feeding structure, the proposed antenna has achieved a wideband dual-CP radiation by a simple combination of a wideband radiator and a conventional hybrid coupler. Although a wider bandwidth and higher gain can be obtained in [26]–[28], but these antennas suffer a more complicated feeding structure, and thus they have a larger size, and higher profile as compared to our proposed design.

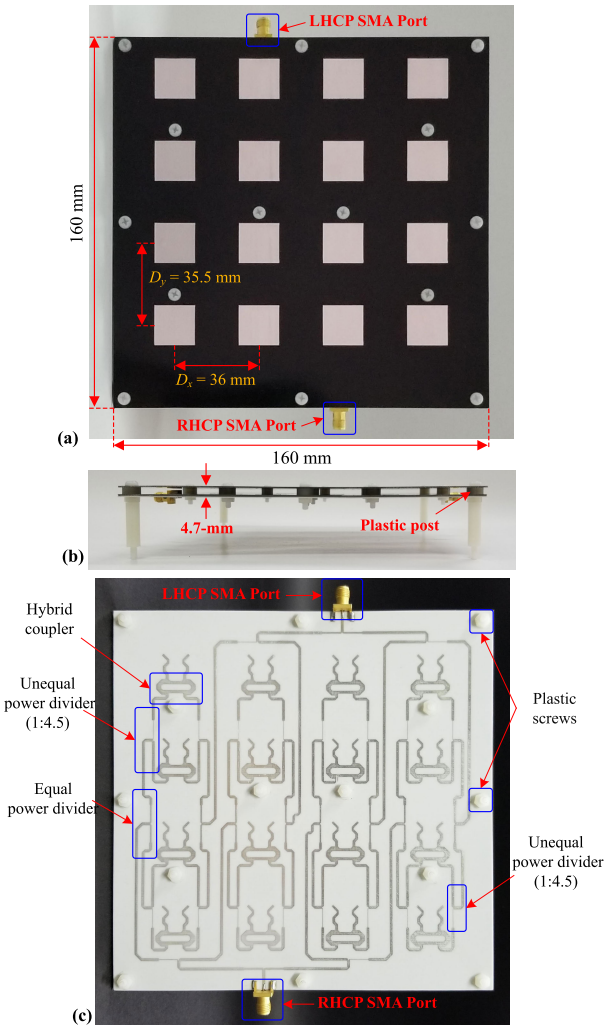

FIGURE 7. A fabricated prototype of 4 × 4 element dual-CP array: (a) top-view, (b) side-view, and (c) bottom-view.

III. DUAL-CIRCULARLY POLARIZED ARRAY

For a more robust dual-CP radiation in terms of high-gain, broad bandwidth, as well as high isolation, the traditional method is to make an array with multiple dual-CP elements [16], [24], [31]–[33]. In our case, the proposed antennas are arrayed in a 4 × 4 layout, as shown in Fig. 7, in which the center-to-center spacing are D_x = 36 mm ($0.6\lambda_0$ at 5-GHz) and D_y = 35.5 mm ($0.59\lambda_0$ at 5-GHz) in the x and y directions, respectively. A feeding network is designed to provide excitation with in-phase and tapered power distribution to achieve a low sidelobe level (SLL). The power distribution ratios are approximately 1 – 4.5 – 4.5 – 1 for exciting the elements along both x and y directions. The feeding network employed quarter-wavelength transformers for impedance matching. The center frequency of 5.5 GHz was chosen for the impedance transformers. The array was first characterized by using the ANSYS Electronics Desktop, and then realized and tested. The array prototype has an overall size of 160 mm × 160 mm × 4.7 mm ($2.47\lambda_{min} \times 2.47\lambda_{min} \times 0.07\lambda_{min}$). The feeding network and two patch

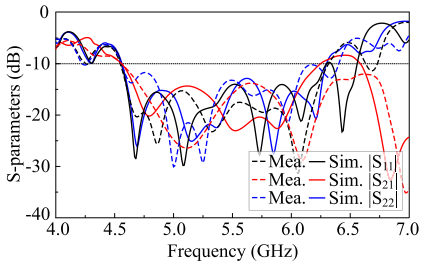

FIGURE 8. S-parameters of the array prototype.

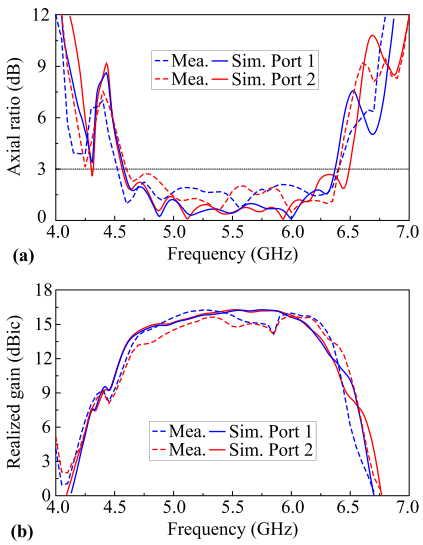

FIGURE 9. a) AR and (b) broadside gain of the array prototype.

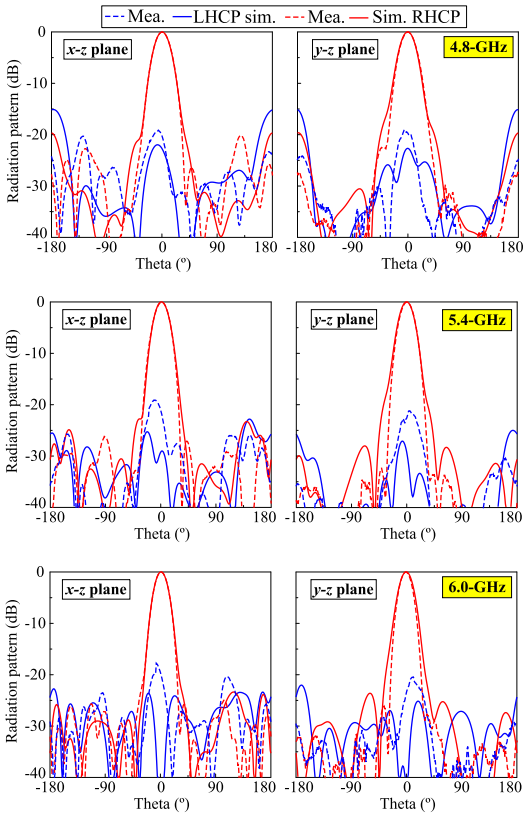

FIGURE 10. Radiation pattern of the array prototype when Port 1 excited.

arrays were realized by using the PCB technology. Being similar to the single-element prototype, the three PCBs of the array were combined by using plastic posts and screws. The simulation and measurement results of the array prototype are compared in Figs. 8−11.

Fig. 8 shows the measured and simulated S-parameters of the array prototype. The impedance-matching bandwidth of the array is similar to that of the single element, which is 32.3% (4.56 – 6.32 GHz) for reflection coefficients (S_{11} and S_{22}) <-10 dB. The port-to-port isolation of the array is greater than that of the single element. The measured isolation was $\geq$14 dB from 4.7 to 6.3 GHz (29.1%), whereas the simulated bandwidth for isolation $\geq$14 dB was 26.6% (4.66 – 6.09 GHz). As mentioned in the case of a single element, a slight discrepancy between the simulated and measured S-parameters of the array could be attributed to some undesired air-gaps between the Sub. 1 and Sub. 2.

Fig. 9 shows the ARs and broadside realized gains of the array prototype. The measurement results agreed rather closely with the ANSYS Electronics Desktop simulations. From Fig. 9(a), the array prototype has achieved a measured 3-dB AR bandwidth of 32.73% (4.6 – 6.4 GHz) for both RHCP and LHCP ports, whereas the simulated value was 32.7% (4.58 – 6.37 GHz). As shown in Fig. 9(b), the array prototype has achieved a measured gain of 12.0 – 16.3 dBic, within the 3-dB AR bandwidth, which is close to the simulation result of 13.0 – 16.3 dBic.

Figs. 10 and 11 show the radiation patterns of the array prototype at 4.8, 5.4, and 6.0 GHz, when the RHCP and LHCP ports are excited, respectively. Again, there is a good agreement between the measurement and simulation results. Across the operational bandwidth, the array prototype has achieved an excellent dual-CP radiation with HPBWs of $24° \pm 2°$ in both $x-z$ and $y-z$ planes, a cross-polarization level of ≤ -16 dB, SLLs <-20 dB, and a F-B ratio of $\geq$25 dB.

The simulated radiation efficiencies (REs) of the array prototype are from 0.6 to 0.7 in the frequency range of 4.7 - 6.0 GHz. These RE values are due to the fact that the patches are built on the low-cost FR4 substrates and the losses are also caused by the feeding network. Higher efficiency can be obtained by using a higher-quality substrate, but the feed losses are still a common shortcoming of the feeding networks based on microstrip-lines [16], [17], [19], [21], [33]. The RE measurements have not been conducted due to the function limitation of the anechoic chamber. Nevertheless, the good agreement between measurement and simulation gains promises a relatively high value of practical RE.

A performance comparison between the proposed design and the previous high-gain dual-CP antennas is given in Table 3. Since the gain is proportional to the number of elements, the larger-size arrays yields higher-gain values.

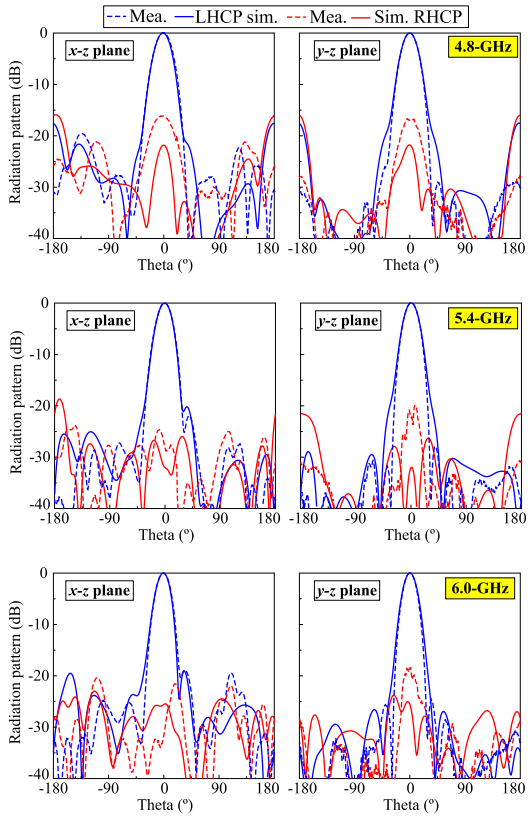

FIGURE 11. Radiation pattern of the array prototype when Port 2 excited.

TABLE 3. Comparison of the high-gain antennas with dual-CP radiation.

Ant.	Size (λ_{min})	Struc.	BW (%)	Iso. (dB)	RE (%)	Gain (dBic)	SLL (dB)
[16]	9.67×9.67 ×0.60	12×12 elem.	50	>20	>50	26.2	<-13
[23]	2.6×2.6 ×0.36	F-P cavity	2.8	>15	N/A	13.4	<-13
[24]	1.23×1.23 ×0.06	2×2 elem.	21.7	>15	N/A	11.2	N/A
[31]	13.0×18.7 ×0.15	2×2 elem.	17	>17	N/A	17.9	<-10
[32]	3.5×2.8 ×0.05	6 elem.	6.6	>20	N/A	11.8	<-13
[33]	1.28×1.28 ×0.14	2×2 elem.	48	>16	>80	14.3	<-10
[34]	5.94×5.94 ×1.0	F-P cavity	2.7	N/A	N/A	19.8	<-16
[35]	4.76×4.76 ×1.52	F-P cavity	4.0	>15	79.3	16.9	<-14
Prop.	2.34×2.34 ×0.07	4×4 elem.	32.7	>14	>60	16.3	<-20

As compared to the antenna arrays that are also realized by the PCB technology [24], [31], [32], the proposed antenna has a comparable low-profile, but has a significantly broader bandwidth. For a 50% bandwidth, the stacked-patch array in [16] employed sequential rotation technique with a multi-layer power distribution network, which increases the profile and complexity significantly. A ME dipole array fed by a 2-section hybrid coupler [33] yields a broader bandwidth than our proposed design does, but it has larger-profile and a more-complicated configuration. The F-P antennas [23], [34], [35] can achieve a high-gain dual-CP radiation with a simple configuration, but they suffer a large-profile and narrow bandwidth. Finally, due to the compact radiator and a fully-optimized feeding network, the proposed antenna has achieved the lowest SLL in comparison with the priors.

IV. CONCLUSION

A low-profile wideband dual-CP antenna and its 4 × 4 element array have been presented. The proposed antenna use a aperture-coupled, stacked patches and a single-section hybrid coupler to achieve the wideband dual-CP radiation. The optimized design has an impedance bandwidth of 30.0% (4.66 – 6.31 GHz), 10-dB isolation bandwidth of 30.9% (4.66 – 6.35 GHz), 3-dB AR bandwidth of 29.1% (4.7 – 6.3 GHz), and a broadside realized gain of 5.5 - 7.05 dBic. The array prototype has achieved a gain of 16.3 dBic, a SLL of ≤ -20 dB, a cross-polarization of ≤ -16 dB, a F-B ratio of ≥ 25 dB, and a port-to-port isolation ≥ 14 dB from 4.7 to 6.3 GHz. With the advantages of low-profile, simple configuration, wideband, dual-CP radiation, and easy fabrication, the proposed antenna design is a good candidate for applications in many wireless communication systems, such as WLAN, satellite communications, synthetic aperture radar, etc.

REFERENCES

[1] S. Gao, Q. Luo, and F. Zhu, *Circularly Polarized Antennas*. New York, NY, USA: Wiley, Nov. 2013.
[2] Z. N. Chen, X. Qing, and H. L. Chung, "A universal UHF RFID reader antenna," *IEEE Trans. Microw. Theory Techn.*, vol. 57, no. 5, pp. 1275–1282, May 2009.
[3] S. X. Ta, H. Choo, I. Park, and R. W. Ziolkowski, "Multi-band, wide-beam, circularly polarized, crossed, asymmetrically barbed dipole antennas for GPS applications," *IEEE Trans. Antennas Propag.*, vol. 61, no. 11, pp. 5771–5775, Nov. 2013.
[4] S. X. Ta, I. Park, and R. W. Ziolkowski, "Circularly polarized crossed dipole on an HIS for 2.4/5.2/5.8-GHz WLAN applications," *IEEE Antennas Wireless Propag. Lett.*, vol. 12, pp. 1464–1467, 2013.
[5] S. X. Ta, V. D. Le, K. K. Nguyen, and C. Dao-Ngoc, "Planar circularly polarized X-band array antenna with low sidelobe and high aperture efficiency for small satellites," *Int. J. RF Microw. Comput.-Aided Eng.*, vol. 29, no. 10, 2019, Art. no. e21914.
[6] S. X. Ta, V. C. Nguyen, K. K. Nguyen, and C. Dao-Ngoc, "Single-feed slotted-patch antenna loaded with metasurface for CubeSat applications," *Int. J. RF Microw. Comput.-Aided Eng.*, vol. 31, no. 4, 2021, Art. no. e22560.
[7] J. T. S. Sumantyo, M. Y. Chua, and C. E. Santosa, "Airborne circularly polarized synthetic aperture radar," *IEEE J. Sel. Topics Appl. Earth Observ. Remote Sens.*, vol. 14, pp. 1676–1692, 2021.
[8] K. P. Liolis, J. Gomez-Vilardebo, E. Casini, and A. I. Perez-Neira, "Statistical modeling of dual-polarized MIMO land mobile satellite channels," *IEEE Trans. Commun.*, vol. 58, no. 11, pp. 3077–3083, Nov. 2010.
[9] D. M. Pozar, "Microstrip antennas," *Proc. IEEE*, vol. 80, no. 1, pp. 79–91, Jan. 1992.
[10] X.-Z. Lai, Z.-M. Xie, Q.-Q. Xie, and X.-L. Cen, "A dual circularly polarized RFID reader antenna with wideband isolation," *IEEE Antennas Wireless Propag. Lett.*, vol. 12, pp. 1630–1633, 2013.
[11] P. Bouca, J. N. Matos, S. R. Cunha, and N. B. Carvalho, "Low-profile aperture-coupled patch antenna array for CubeSat applications," *IEEE Access*, vol. 8, pp. 20473–20479, 2020.
[12] P. Squadrito, S. Zhang, and G. F. Pedersen, "X-band dual circularly polarized patch antenna with high gain for small satellites," *IEEE Access*, vol. 7, pp. 74925–74930, 2019.

[13] E. Aloni and R. Kastner, "Analysis of a dual circularly polarized microstrip antenna fed by crossed slots," *IEEE Trans. Antennas Propag.*, vol. 42, no. 8, pp. 1053–1058, Aug. 1994.
[14] A. Narbudowicz, X. Bao, and M. J. Ammann, "Dual circularly-polarized patch antenna using even and odd feed-line modes," *IEEE Trans. Antennas Propag.*, vol. 61, no. 9, pp. 4828–4831, Sep. 2013.
[15] E. Zhang, A. Michel, M. R. Pino, P. Nepa, and J. Qiu, "A dual circularly polarized patch antenna with high isolation for MIMO WLAN applications," *IEEE Access*, vol. 8, pp. 117833–117840, 2020.
[16] A. Garcia-Aguilar, J. M. Inclan-Alonso, L. Vigil-Herrero, J. M. Fernandez-Gonzalez, and M. Sierra-Perez, "Low-profile dual circularly polarized antenna array for satellite communications in the X band," *IEEE Trans. Antennas Propag.*, vol. 60, no. 5, pp. 2276–2284, May 2012.
[17] C. Zhang, X. Liang, X. Bai, J. Geng, and R. Jin, "A broadband dual circularly polarized patch antenna with wide beamwidth," *IEEE Antennas Wireless Propag. Lett.*, vol. 13, pp. 1457–1460, 2014.
[18] H. H. Tran, N. Nguyen-Trong, and H. C. Park, "A compact dual circularly polarized antenna with wideband operation and high isolation," *IEEE Access*, vol. 8, pp. 182959–182965, 2020.
[19] Y. Shen, S.-G. Zhou, G.-L. Huang, and T.-H. Chio, "A compact dual circularly polarized microstrip patch array with interlaced sequentially rotated feed," *IEEE Trans. Antennas Propag.*, vol. 64, no. 11, pp. 4933–4936, Nov. 2016.
[20] R. Ferreira, J. Joubert, and J. W. Odendaal, "A compact dual-circularly polarized cavity-backed ring-slot antenna," *IEEE Trans. Antennas Propag.*, vol. 65, no. 1, pp. 364–368, Jan. 2017.
[21] S. J. Chen, C. Fumeaux, Y. Monnai, and W. Withayachumnankul, "Dual circularly polarized series-fed microstrip patch array with coplanar proximity coupling," *IEEE Antennas Wireless Propag. Lett.*, vol. 16, pp. 1500–1503, 2017.
[22] Z. Wu, M.-C. Tang, T. Shi, and R. W. Ziolkowski, "Two-port, dual-circularly polarized, low-profile broadside-radiating electrically small Huygens dipole antenna," *IEEE Trans. Antennas Propag.*, vol. 69, no. 1, pp. 514–519, Jan. 2021.
[23] Y. Wang and A. Zhang, "Dual circularly polarized Fabry–Pérot resonator antenna employing a polarization conversion metasurface," *IEEE Access*, vol. 9, pp. 44881–44887, 2021.
[24] W. Yang, Q. Meng, W. Che, L. Gu, and Q. Xue, "Low-profile wideband dual-circularly polarized metasurface antenna array with large beamwidth," *IEEE Antennas Wireless Propag. Lett.*, vol. 17, no. 9, pp. 1613–1616, Sep. 2018.
[25] S. Liu, D. Yang, and J. Pan, "A low-profile broadband dual-circularly-polarized metasurface antenna," *IEEE Antennas Wireless Propag. Lett.*, vol. 18, no. 7, pp. 1395–1399, Jul. 2019.
[26] H. H. Sun, H. Zhu, C. Ding, and Y. J. Guo, "Wideband planarized dual-linearly-polarized dipole antenna and its integration for dual-circularly-polarized radiation," *IEEE Antennas Wireless Propag. Lett.*, vol. 17, no. 12, pp. 2289–2293, Dec. 2018.
[27] H. Govindarajan, S. C. Pavone, L. D. Donato, P. D. Mariano, G. Distefano, P. Livreri, P. Nagaradjane, C. Squadrito, and G. Sorbello, "Design of a compact dual circular-polarized antenna for L-band satellite applications," *IEEE Antennas Wireless Propag. Lett.*, vol. 19, no. 4, pp. 547–551, Apr. 2020.
[28] W. Chen, Z. Yu, J. Zhai, and J. Zhou, "Developing wideband dual-circularly polarized antenna with simple feeds using magnetoelectric dipoles," *IEEE Antennas Wireless Propag. Lett.*, vol. 19, no. 6, pp. 1037–1041, Jun. 2020.
[29] D. M. Pozar, *Microwave Engineering*. Hoboken, NJ, USA: Wiley, 2012, p. 343.
[30] S. D. Targonski, R. B. Waterhouse, and D. M. Pozar, "Design of wide-band aperture-stacked patch microstrip antennas," *IEEE Trans. Antennas Propag.*, vol. 46, no. 9, pp. 1245–1251, Sep. 1998.
[31] J. Zhu, S. Liao, Y. Yang, F. Li, and Q. Xue, "60 GHz dual-circularly polarized planar aperture antenna and array," *IEEE Trans. Antennas Propag.*, vol. 66, no. 2, pp. 1014–1019, Feb. 2018.
[32] Y.-H. Yang, B.-H. Sun, and J.-L. Guo, "A low-cost, single-layer, dual circularly polarized antenna for millimeter-wave applications," *IEEE Antennas Wireless Propag. Lett.*, vol. 18, no. 4, pp. 651–655, Apr. 2019.
[33] B. Feng, L. Li, K. L. Chung, and Y. Li, "Wideband widebeam dual circularly polarized magnetoelectric dipole antenna/array with meta-columns loading for 5G and beyond," *IEEE Trans. Antennas Propag.*, vol. 69, no. 1, pp. 219–228, Jan. 2021.
[34] M. U. Afzal, A. Lalbakhsh, and K. P. Esselle, "Method to enhance directional propagation of circularly polarized antennas by making near-electric field phase more uniform," *IEEE Trans. Antennas Propag.*, vol. 69, no. 8, pp. 4447–4456, Aug. 2021.
[35] Y.-L. Li and K.-M. Luk, "Dual circular polarizations generated by self-polarizing Fabry–Pérot cavity antenna with loaded polarizer," *IEEE Trans. Antennas Propag.*, vol. 69, no. 12, pp. 8890–8895, Dec. 2021.

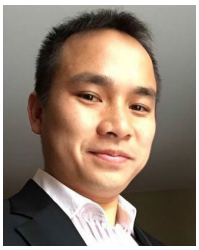

SON XUAT TA received the B.Sc. (Eng.) degree in electronics and telecommunications from the Hanoi University of Science and Technology, Vietnam, in August 2008, and the Ph.D. degree in electrical engineering from Ajou University, South Korea, in February 2016. From March 2016 to February 2017, he was a Postdoctoral Research Fellow with the Department of Electrical and Computer Engineering, Ajou University. From March 2017 to August 2017, he was with the Division of Computational Physics, Institute for Computational Science, and the Faculty of Electrical and Electronics Engineering, Ton Duc Thang University, Ho Chi Minh City, Vietnam. Since September 2017, he has been working as a Lecturer at the School of Electronics and Telecommunication, Hanoi University of Science and Technology. He has authored or coauthored over 90 technical journals and conference papers. His research interests include antennas, metamaterials, metasurfaces, metamaterial-based antennas, metasurface-inspired antennas, circularly polarized antennas, and millimeter-wave antennas. He has served as a reviewer for over 15 scientific journals.

VAN CUONG NGUYEN received the B.Sc. (Eng.) and M.Sc. degrees in electronics and telecommunication from the Hanoi University of Science and Technology, Hanoi, Vietnam, in 2019 and 2021, respectively, where he is currently pursuing the Ph.D. degree in electromagnetic field and microwave technology with the Communication Research and Development Laboratory. His research interests include CubeSat antenna, reflectarray antenna, MIMO antenna, phased array antenna, and full-duplex antenna.

BANG-TAM NGUYEN-THI is currently pursuing the B.Sc. (Eng.) degree in electronics and telecommunications with the Hanoi University of Science and Technology (HUST), Vietnam. Since 2020, she has been working as an Internship Researcher at the Communication Research and Development Laboratory, HUST. Her research interests include patch antennas, dual circularly polarized antennas, and wideband antennas.

THAI BAO HOANG received the B.Sc. (Eng.) degree in electronics and telecommunications from the Hanoi University of Science and Technology (HUST), Vietnam, in 2021. He is currently a Graduate Student majoring in telecommunications technology with the HUST. He is also studying and researching at the Communication Research and Development Laboratory, HUST. His research interests include metasurface, coding metasurface, optimization algorithms, and metamaterial-based antenna.

AN NGOC NGUYEN (Member, IEEE) was born in Hanoi, Vietnam, in December 1988. He received the B.E. degree in telecommunication engineering from the Hanoi University of Science and Technology, in 2011, and the M.E. and Ph.D. degrees in electrical, electronic and communication engineering from Chuo University, Japan, in 2014 and 2017, respectively. Since April 2017, he has been with the University of Engineering and Technology-VNU, Hanoi, where he is currently a Lecturer. His current research interests include smart sensors, and antenna and material characterization using free space techniques.

KHAC KIEM NGUYEN was born in Hanoi, Vietnam, in 1978. He received the B.Eng., M.Sc., and Ph.D. degrees from the School of Electronics and Telecommunication (SET), Hanoi University of Science and Technology (HUST), Vietnam, in 2001, 2003, and 2017, respectively. Since 2001, he has been working as a Lecturer at the SET, HUST, and a Researcher at the CRD Laboratory, HUST. His research interests include design microstrip antenna for next generation mobile communication systems as well as passive RF components.

CHIEN DAO-NGOC (Senior Member, IEEE) received the Dipl.Eng. degree from the School of Electronics and Telecommunication (SET), Hanoi University of Science and Technology (HUST), Vietnam, in 1997, and the M.Sc. and Ph.D. degrees from the Department of Electronics and Computer Engineering, Gifu University, Japan, in 2002 and 2005, respectively.

From April 2005 to October 2011, he worked as a Senior Lecturer at the SET, HUST, and appointed as the Director of the Centre for Research and Development on Satellite Navigation Technology, South East Asia, in 2009. He has been appointed as an Associate Professor, since November 2010. Since November 2011, he has been with the Department of High Technology, Ministry of Science and Technology, Vietnam, and appointed as an Adjunct Professor at the SET, HUST. His research interests include computational electromagnetics based on MoM and FDTD method, analysis and design of modern antenna, and nanometric integrated optical circuits based on surface plasmon polaritons.

Dr. Dao-Ngoc has been a Reviewer for several journals/transactions of Optical Society of America (OSA), IEEE, Elsevier, and American Geophysical Union (AGU) as well as numerous of technical and science conferences.